92_Revisi_2.0.docx

by

Submission date: 31-May-2023 02:15PM (UTC+0700)
Submission ID: 2105838119
File name: 92_Revisi_2.0.docx (4.24M)
Word count: 5205
Character count: 28381

Performance comparison for Hearth Rate Signal Detection for Different location in Fingertip and wrist using sensor MAX30102

Rohmat Gunawan[1,a], Asep Andang[2,b*], Muhammad Ridwan[2,c]

[1]Department of Informatics, Universitas Siliwangi, Jl. Siliwangi No. 24, Tasikmalaya, 46115, Indonesia

[2,4]Department of Electrical Engineering, Universitas Siliwangi, Jl. Siliwangi No. 24, Tasikmalaya, 46115, Indonesia

[a]rohmatgunawan@unsil.ac.id, [b*]andhangs@unsil.ac.id, [c]muhamadridwan@student.unsil.ac.id

Keywords: max30102, heart rate, wrist, fingertip, detrend.

Abstract. Measuring vital body signals is essential to measure basic body functions, prevent misdiagnosis, detect underlying health problems and motivate healthy lifestyle changes. Vital body signals are measured at the fingertips because the skin is thin, and the blood vessels are transparent. Visible light is passed at the fingertips, and the pulses generated are still acceptable on the outer nail. However, the body's vital signal measuring device continuously attached to the fingertip causes discomfort to the user. Therefore, in this study, it is proposed to measure the body's vital signals in other body parts. The wrist was chosen to be attached to the body's vital signal measuring device because the measuring device attached to the wrist allows it to continue to be used. This study aims to measure the body's vital signals, especially heart rate, on the wrist so that the correlation level of the measurement data is known. The MAX30102 sensor, which uses visible light with 650 - 670 nm, was selected for measurement. The ratio of the light reflected through the fingertips compared to the wrist. The result of measuring the heart rate signal on the wrist is in the form of a relatively flat wave so that the data sharpening process is carried out using the detrend method. The results showed that the measurement of heart rate signals at the wrist and fingertips of 15 respondents had accuration 85%. The accuration value shows that the data from the heart rate signal at the wrist is closely correlated with the data from the measurement of the heart rate signal at the fingertips. Therefore, measurements of heart rate signals, usually performed on the fingertips, can also be performed on the wrist. From the test results with a strong accuration, measurements are always taken when the hand can measure the place to measure vital signals, which is usually done at the fingertips.

Introduction

The development of the instrument and electronic technology significantly contributes to observing various natural phenomena and phenomena in various fields, including industry, telecommunications, and health. One of the implementations of instrumentation technology that utilizes light sensors with variations in wavelength is the measurement of the body's vital signals. Measuring vital signals in the body is essential for measuring basic body functions, preventing misdiagnosis, detecting underlying health problems, and motivating healthy lifestyle changes.

Based on the study's results, variations in the wavelengths emitted by laser light on the body can penetrate the skin at different depths resulting in different effects. One of the rays used in measuring vital body signals is an Infra Red-Light Emitting Diode (IR LED) with a wavelength of 760 nm to 100,000 nm. IR LEDs are grouped into Near IR LEDs (NIR LEDs) with a wavelength of 780 nm - 3,000 nm, Middle IR LEDs (MIR LEDs) with a wavelength of 3,000 nm - 50,000 nm, and Far IR LEDs (FIR LEDs) with a wavelength of 50,000 nm - 100,000 nm [1].

During the COVID-19 pandemic, thermography which applies IR technology to detect the thermal distribution of an object, is widely used to detect human body temperature [2][3]. MIR LEDs have been successfully applied in research for (1) quantification of clinical parameters in body fluids, (2) diagnosis and monitoring of cancer and other diseases by analysis of body fluids, cells, and tissues,

and (3) classification of clinically relevant microorganisms, and (4) analysis of kidney stones, nails, and faecal fat[4] MIR LED use to exhaled breath analysis[5].

MIR LEDs also allow for the detection of blood glucose levels [6]. Several studies have also succeeded in applying NIR LEDs to brain activities such as autism spectrum disorder, attention-deficit hyperactivity disorder, epilepsy, depressive disorders, anxiety and panic disorder, schizophrenia, mild cognitive impairment, Alzheimer's disease, Parkinson's disease, stroke[7], and traumatic brain injury[8][9]. NIR-LED is also widely used in detecting the body's blood sugar level [10]–[12]. NIR LED are also used for non-invasive measurement of right atrial pressure [13], cardiovascular[14][15], heart rate[16]–[18] and blood pressure[19]–[22].

The use of IR in detecting vital body signals continues to grow, including using the Photoplethysmograph (PPG) method.[23]–[25]. Works based on pulse oximetry light method. PPG can be reflected or transmitted through skin, bone, or tissue. The original light emitted by the LED, IR, NIR, and MIR, penetrates the skin layer and is then reflected on the skin surface where the photodiode will receive it. The photodiode will measure the intensity of the light it receives and convert it into an electric current[26].

Various PPG-based studies involving infrared were carried out using different wavelengths. Hina uses the PPG method with NIR LED wavelengths of 1070nm, 950nm, and 935nm[27]. Then at 1850 nm, 1710 nm, 1520 nm, and 1200 nm [28].

IR emitted to the body will be transmitted and reflected to produce various data that can be used to analyze health conditions. Experiments on measuring the body's vital signals have been carried out in several different parts of the body, including fingertips[29], wrists[30], ear lobes[31], and arms[32]. Measurements from various body parts produce advantages and disadvantages related to accuracy, comfort, and function[33]. Measurement of vital body signals is often done at the fingertips because the fingertips are the thinnest part of the body. There are many nerve endings, and the light emitted can penetrate the nails[34].

However, the tool for measuring vital body signals at the fingertips that are continuously attached will cause inconvenience to the user. In addition to the fingertips, the wrists are other body parts widely used to measure the body's vital signals. The wrist was chosen to be tested in this study because the measuring device attached to the wrist allows it to be used continuously and is more convenient to wear[35]. The wrist is another body part that can place a sensor measuring vital body signals embedded in the watch. The implementation of the body signal measuring sensor on this watch produces a smart wearable device, making it a multi-functional device[36]. A smartwatch, which allows it to be used continuously throughout the day, has been used to obtain vital body signal data from sensors mounted on the bottom of the watch[37].

The main novelty of this research is built an electronic system to measure vital body signals, especially heart rate at the wrist with the help of the MAX30102 sensor that uses visible light with 650 - 670 nm.

Skin thickness, different skin pigment colours, and stability during data collection, because the hand is one of the most active parts of the body, are some of the conditions that can affect the process of measuring the body's vital signals. The unknown accuracy of the measurement results of the body's vital signals at the wrist is one of the exciting problems to be studied. Therefore, in this study, the body's vital signals will be measured at the wrist and the fingertips. The data from measuring the body's vital signals at the wrist and fingertips will be recorded in a table, and the correlation value will be calculated.

Methods

In this study, the ability to process analog to digital from the MAX30102 is influenced by the ADC resolution of 18bit. So, the conversion of the ADC value to voltage can be seen as follows in equation (1).

$$V_{adc} = \frac{ADC_{value}}{2^{18} - 1} x\, V_s \quad (1)$$

Where V_{adc} is the conversion voltage from the input ADC value. Then the ADC value is the value derived from the PPG signal and *Vs* is the MAX30102 source voltage. Meanwhile, to calculate the Heart Bit Rate (HBR) for 10 seconds can use equation (2).

$$\text{HBR} = \frac{60 \text{ x } P_{10}}{T_s} \tag{2}$$

Where *Ts* is the sampling time for 10 seconds and P_{10} is pulse for 10 seconds. The schematic of the heart bit rate using electronic circuit can be seen in Fig. 1.

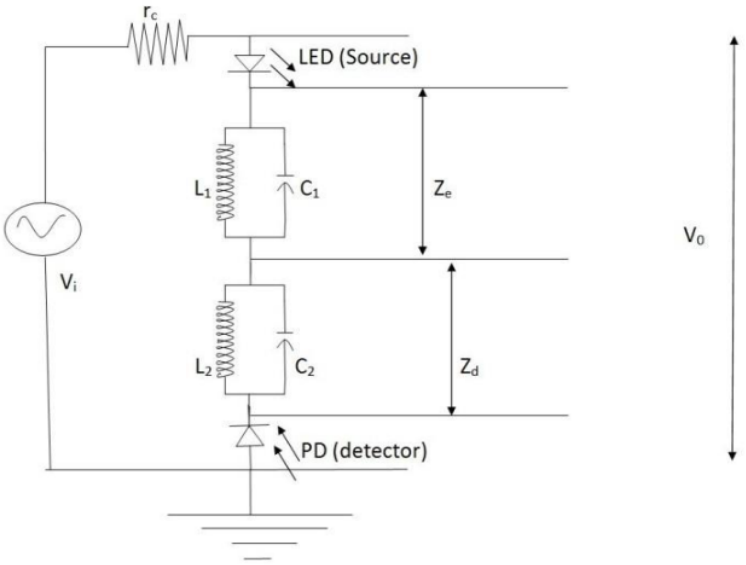

Fig. 1. PPG circuit for the heart beat [38]

The following equations were generated from the suggested electrical equivalent circuit (See Fig. 1) [38].

$$\text{Ze(s)} = \frac{\text{SL}_1}{1+s^2L_1C_1} \tag{3}$$

$$\text{Zd(s)} = \frac{\text{SL}_2}{1+s^2L_2C_2} \tag{4}$$

$$\text{Z(s)} = Z_e(s) + Z_d(s) \tag{5}$$

$$\text{Z(s)} = \left(\frac{\text{SL}_1}{1+s^2L_1C_1} + \frac{\text{SL}_2}{1+s^2L_2C_2}\right) \tag{6}$$

$$V_0(\text{s}) = I(s)\text{Z}(s)$$

where,

$$\text{I(s)} = \frac{V_i(s)-V_0(s)}{r_c} \tag{7}$$

$$V_0(\text{s}) = \left(\frac{V_i(s)-V_0(s)}{r_c}\right)Z(s) \tag{8}$$

$$V_0(\text{s}) = \left(\frac{V_i(s)-V_0(s)}{r_c}\right)\left(\frac{\text{SL}_1}{1+s^2L_1C_1} + \frac{\text{SL}_2}{1+s^2L_2C_2}\right) \tag{9}$$

$$V_0(\text{s})\left(\frac{1}{r_c}\right) = \left(\frac{\text{SL}_1}{1+s^2L_1C_1} + \frac{\text{SL}_2}{1+s^2L_2C_2}\right)\left(\frac{V_i(s)}{r_c}\right) \tag{10}$$

$$\frac{V_0(s)}{V_i(s)} = \left(\frac{\left(\frac{\mathrm{SL}_1}{1 + s^2 L_1 C_1} + \frac{\mathrm{SL}_2}{1 + s^2 L_2 C_2} \right)}{(1 + r_c)} \right) \tag{11}$$

Since $(1 + r_c)$ is constant so $\frac{1}{(1+r_c)} = k$; we get

$$\frac{V_0(s)}{V_i(s)} = k \left(\frac{\mathrm{SL}_1}{1 + s^2 L_1 C_1} + \frac{\mathrm{SL}_2}{1 + s^2 L_2 C_2} \right) \tag{12}$$

For unit step response $V_i(s) = \frac{1}{s}$, we obtained

$$V_0(s) = k \left(\frac{\mathrm{L}_1}{1 + s^2 L_1 C_1} + \frac{\mathrm{L}_2}{1 + s^2 L_2 C_2} \right) \tag{13}$$

$$V_0(s) = k \left(\frac{\mathrm{L}_1 C_1}{C_1 (1 + s^2 L_1 C_1)} + \frac{\mathrm{L}_2 C_2}{C_2 (1 + s^2 L_2 C_2)} \right) \tag{14}$$

Taking Inverse Laplace Transform;

$$V_0(t) = k \left(\frac{\sin \mathrm{w}_1(t)}{C_1} + \frac{\sin \mathrm{w}_2(t)}{C_2} \right) \tag{15}$$

where,

$$w_1(t) = \sqrt{L_1 C_1} \text{ and } w_2(t) = \sqrt{L_2 C_2}$$

Since the heartbeat and the ac component of the PPG signal are synced, we know that the heartbeat is periodic. As a result, L_2 and C_2 should have values that $w_1 = 0.5 w_2$. So now the equation becomes [38].

$$V_0(t) = k \left(\frac{\sin w\, t}{C_1} + \frac{\sin 2w\, t}{C_2} \right) \tag{16}$$

where $V_0(\mathrm{t})$is the output voltage in volts. Ignore the "Z" since the Z value will be very high because the inductors are measured in millihenry (mH) and the capacitors are measured in pico Farad (pF).

Tests were carried out using the MAX 30102 sensor to determine the signals generated by the body from both the fingers and the wrist. This MAX30102 sensor is attached to the LILYGO®TTGO. The LED MAX 30102 sensor consists of 2 pieces: a visible red LED with a wavelength of 660 nm and an infrared LED with a wavelength of 880 nm[39]. This LED sensor is used for High-Sensitivity Pulse Oximeter and Heart-Rate Sensor for Wearable Health[40]. This sensor is connected to the ESP32 as a microcontroller unit that displays, processes, and manages incoming data. Fig. 2 shows the circuit of MAX30102 connecting to ESP32.

The MAX 30102 sensor is embedded in the watch so that it is easy to use for detecting vital body signals because it is in direct contact with the wrist's skin. MAX30102 is also used to get a PPG signal[41].

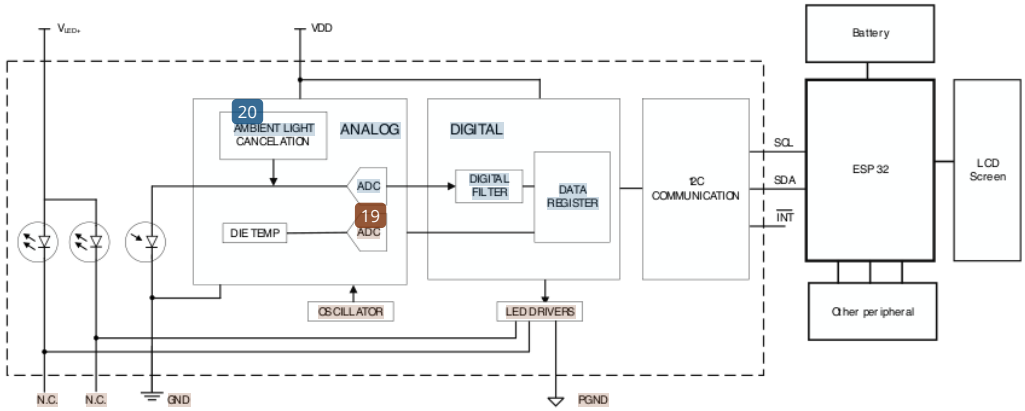

Fig.2 Connection MAX30102 and ESP 32

On the LILYGO®TTGO smartwatch, the MAX30102 sensor is placed at the bottom. The LCD screen is at the top so that the measurement data can be easily seen. Measurements are carried out in two different positions, first by placing the fingertip above the MAX 30102 sensor for approximately 3 minutes, the second by placing the MAX 30102 sensor on the wrist or using it as a watch and positioned silently in the plane of arrival parallel to the elbow for approximately 3 minutes. The sampling process is shown in Fig. 3.

In Fig. 3(a), the test is carried out on the fingertips. In Fig. 3(b), the test is carried out on the arm. Respondents involved in the sampling amounted to 15 people. The respondents have age variations ranging from 20 s.d. 46 years, with an unregulated gender ratio of women and men. The test was performed five times, and the graph with the best stability in its waveform was taken.

(a) Fingertip Measurement

(b) Wrist Measurement

Fig. 3 Signal data retrieval

The detrend process can be seen in the flowchart in Fig. 4. The process begins with reading the ADC value from the MAX 30102 signal in *.xlsx data format for 10 seconds. The results show data per second as much as 37 points/second or 370 points per 10 seconds. The next step is to determine the waveform. The number of waves is determined manually by looking at the ppg wave plot and counting the number of waves—the more samples for one wave, the lower the frequency of the PPG wave. On the contrary, the fewer samples for one wave, the higher the frequency of the PPG wave.

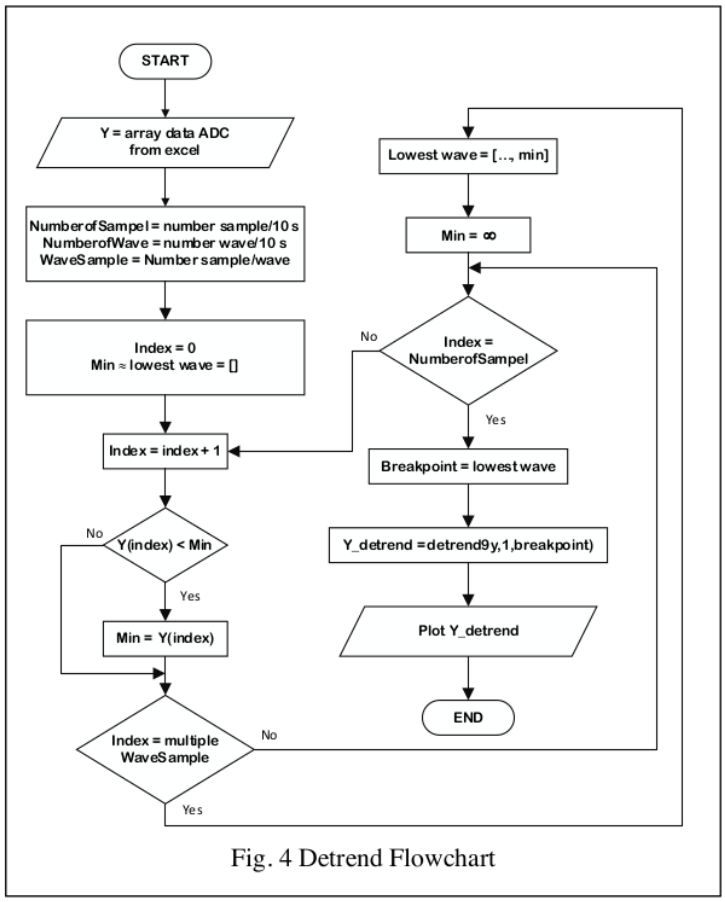

Fig. 4 Detrend Flowchart

A breakpoint is needed to carry out the detrending process, where the breakpoint is the boundary point of a linear wave. A breakpoint is the maximum or minimum value of a wave, where this breakpoint is a linear wave boundary without oscillation. Getting a breakpoint on data containing many samples representing the wave function value requires an iteration technique. The lowest values or valleys of PPG waves can be known with iteration.

The iteration process follows the flowchart in Figure 4. This iteration process is carried out to obtain the minimum values per period, which are the parameters of the PPG signal. Before performing the initialization iteration, setup is done on the index variable with a value of 0, the minimum value is infinite, and the wave valley is an empty array. As the iteration progresses, the wave valleys will be filled with breakpoints (wave valleys). Each iteration will check whether the value of Y with the current index is less than the minimum value. The minimum value equals Y with the current index if it is smaller than the minimum value. Iteration will also be checked whether the iteration has carried out the iteration process as many as multiples of the wave sample. If true, the wave trough array variable is added to the minimum value variable data. After that, the minimum value is reset back to infinity. So that every single wave trough variable gets a new minimum value or breakpoint after the

index is equal to many samples, it indicates the iteration process is complete, and the breakpoint for the detrending process is ready to be used. Detrend was also carried out on the Y variable with the detrend type, linear, and breakpoint from the wave valley variable.

This algorithm is simulated with Matlab. By default, Matlab has a detrend function but is limited to linear detrending (piece-wise) by subtracting from the data the least squares match result from a straight line to the data [42]. Therefore, the detrend algorithm was created manually, and the input data comes from a file with *.xlsx format.

Result

In this work, the normality of the data distribution was tested using the Shapiro Wilk test because the number of samples was small (<50). The results of the Shapiro Wilk test show that the *p* value for the fingertips variable is 0.973, which means that the data is normally distributed. The wrist variable *p* value is 0.011, which means that the data is not normally distributed (See Table 1). Because there is one variable that is not normally distributed, the different test uses the Mann Whitney test.

Table. 1 Test of Normality

	Test Normality					
	Statistics	df	Sig.	Statistics	df	Sig.
Fingertip	0.145	15	0.200*	0.981	15	0.973
Wrist	.250	15	0.012	0.837	15	0.011

*. This is a lower bound of the true significance
a. Lilliefors Significance Correction

Next, we carry out further verification with a different test. The Mann Whitney test results obtained pValue of 0.76 meaning that there is no difference in the results of the tests carried out at the fingertips and wrist. The Mann Whitney test can be seen in Table 2.

Table 2. The Mann Whitney test

ar Test
Mann Whitney test

	Rank			
	Checkpoint	N	Mean Rank	Sum of Rank
Results	Fingertip	15	15.97	239.50
	Wrist	15	15.03	225.50
	Total	30		

Test Statistics	Results
Mann Whitney U	105.500
Wilcoxon W	225.500
Z	-0.294
Asym.sig (2 tailed)	0.769
Exact Sig. (2*(1 tailed sig))	0.775[b]

a. Grouping variables: Checkpoint
b. Not Corrected for Ties

The data from the signal measurement at the fingertips produces a more stable waveform than the data from the signal measurement at the wrist, as shown in Fig. 5. The stable signal is made stable by eliminating oscillatory interference. This oscillation occurs due to external disturbances such as unwanted arm movement or the condition of the respondent's activities that interfere with the signal. A wave engineering process called detrend carried out to eliminate the oscillation. Detrend is smoothing wave crests and troughs with the same peak-to-peak value. Detrended fluctuation analysis (DFA) is an effective model for measuring non-stationary time series autocorrelation. It is mainly used to minimize the influence of external trends on autocorrelation by calculating detrended fluctuations [43]. This DFA process is also carried out in PPG signals for skin blood pulsation and Electrocardiographic[44][45]. The wave oscillation due to instability can be seen in Fig. 6.

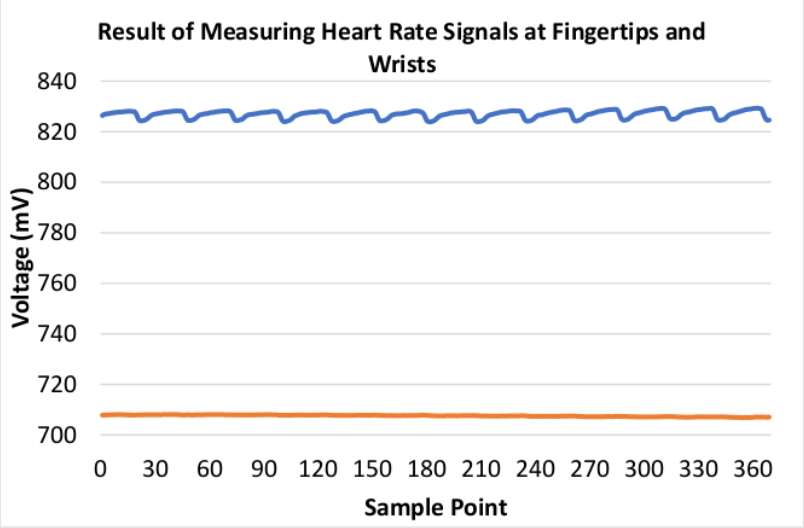

Fig. 5 Comparison of measurements on finger and wrist

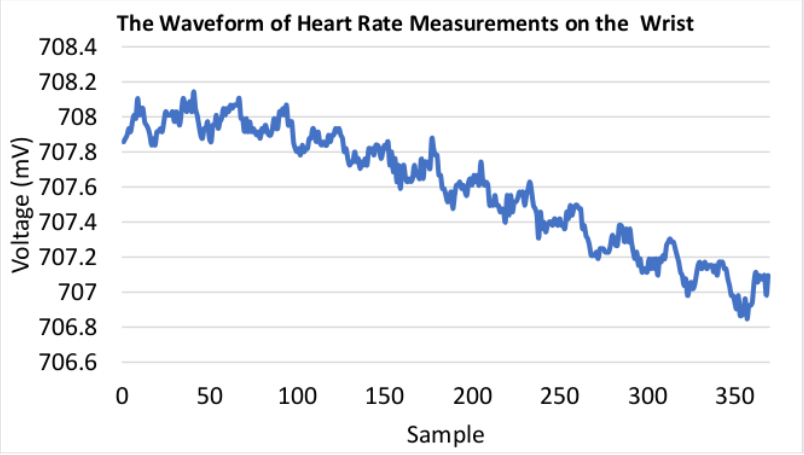

Fig. 6 Data oscillation on the wrist

Figure 7(a) shows the PPG signal with 370 data samples on the first respondent's finger. With a sampling rate of 37 per second, the selected data represents the measurement for 10 seconds. This shows that the 14 wave crests on the graph determine the respondent's heart rate in 10 seconds. This ppg signal capture on the finger has minimal noise but has a fluctuating offset. Meanwhile, Figure 7 (b) shows the results of the detrend process in Matlab to eliminate offsets in Figure 7 (a). After the detrend offset process on the wave, the signal has a more constant characteristic and the wave crest does not change.

Figure 7 (c) shows the ppg signal with 370 data samples on the wrist of the first respondent. With a sampling rate of 37 per second, the selected data represents the measurement for 10 seconds. This means that 13.5 wave crests on the graph determine the respondent's heart rate in 10 seconds. The ppg signal capture on the wrist has more noise than the finger ppg signal in Figure 7 (a) and the offset tends to be linear down. Meanwhile, Figure 7(d) presents the results of the detrend process in Matlab to eliminate offsets in Figure 7(c). After the detrend offset process on the wave, the signal becomes much more constant horizontally and the number of wave crests does not change, which is 13.5.

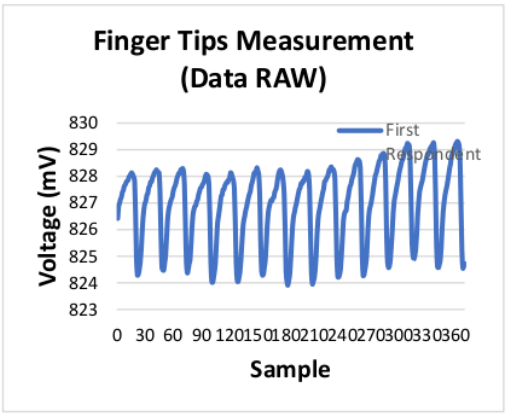

(a) Fingertips Measurement (Data RAW)

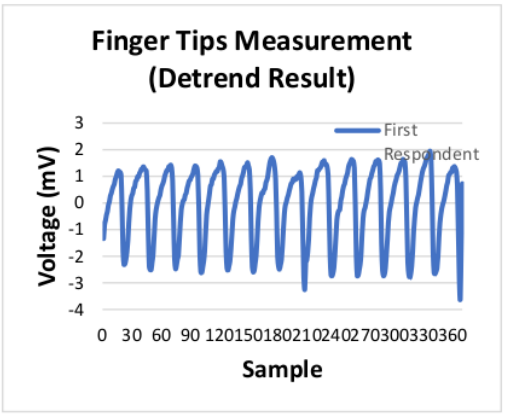

(b) Finger Tips Measurement (Detrent Result)

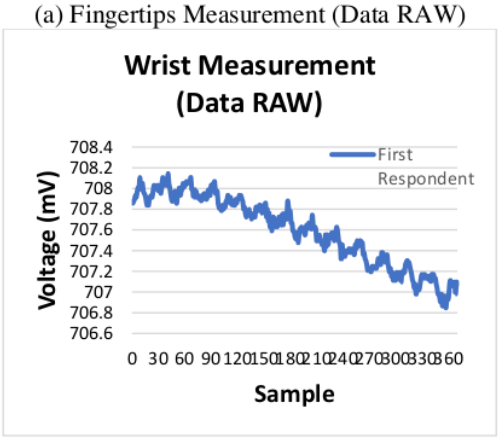

(c) Wrist Measurement (Data RAW)

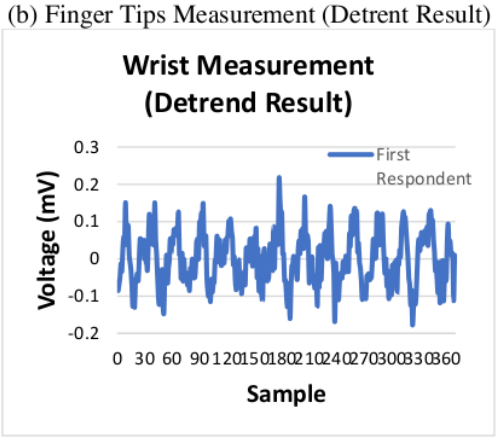

(d) Wrist Measurement (Detrent Result)

Fig. 7 The process of changing waves using detrend first and third respondent

Table 3. Results of measuring wave period of a heartbeat at the fingertips and wrist

No	Number of Waves	
	Fingertips	Wrist
1	14.00	13.50
2	14,00	14.00
3	15.00	14.00
4	15.00	16.00
5	14.50	14.50
6	13.00	14.00
7	14.50	13.00
8	13.50	14.00
9	14.00	13.50
10	17.00	17.00
11	15.00	14.50
12	16.00	16.50
13	12.50	13.00
14	13.50	13.50
15	11.50	13.00
Correlation		**0.82**

The data displayed shows 3 of the 15 respondents described previously. The process carried out on these three respondents represents the process on all respondents automatically using the algorithm described previously, which produces data according to Table 3.

Discussion

The detrend process or signal wave improvement has been carried out by measuring the body's vital signals at the fingertips and wrists using the MAX30102 sensor. The calculation results show that the measurement of signals on the wrist and fingertips with 15 respondents has a accuration value of 82%. Therefore, vital signal measurements, usually performed at the fingertips, can also be performed at the wrist.

From the results of detrend using Matlab, the results of taking data from the fingertips are equal to data from getting hands. This detrend process is carried out numerically with the algorithm in Figure 5 and Figure 7. The drawback is that the signal must be converted based on time units and saved in csv or xlsx format to produce a detrend process causes the detrend process cannot be carried out immediately, it takes a process to convert the detected signal into an xlsx or CSV file.

Rajala [46]compares the wrist and fingertip PPG signals. The process proves that the fingertip's value is greater than the wrists. Test one also compares the different PATs between fingertips and wrists but does not discuss the detrend process to determine the number of valleys of the studied signal period. Tsai [47] performed the decomposition process of PPG signals originating from the wrist and fingertips with the variant method of Pulse Decomposition Analysis by analyzing them one by one to obtain a significant correlation between signals from the wrist and fingers.

The obstacle in this implementation is the limited number of respondents because it is still in a covid situation, so it is pretty complex that the number of respondents is limited.

The results of the research carried out strengthen the assumption that one day with data engineering with ppg signal processing on the MCU portable, the signal from the wrist will be able to match the signal from the finger, and measurements can be carried out continuously without impeding human movement, and user comfort can be protected.

Conclusion

The main novelty of this research is built an electronic system to measure vital body signals, especially heart rate at the wrist based on the MAX30102 sensor that uses visible light with 650 - 670 nm. The detrend process is carried out to equalize the data using Matlab. The results showed that the measurement of heart rate signals at the wrist and fingertips of 15 respondents had accuration 85%.

The results of the data engineering process obtained a linear signal so that the result is a comparative calculation of the signal period from the fingertips and wrist. The comparison process results in a close relationship between signal periods from the fingertips and wrist.

This result reinforces the notion that signals from the wrist have the same significance as signals from the fingertips. In the future, data retrieval can be done simply from the wrist so that it does not interfere with the wearer's activities and work comfort.

Acknowledgement

This research is a grant from the Ministry of Education, Culture, Research, And Technology of the Republic of Indonesia with contract number 243/E5/PG.02.00.PT/2022.

References

[1] F. Vatansever and M. R. Hamblin, "Far infrared radiation (FIR): its biological effects and medical applications.," *Photonics Lasers Med.*, vol. 4, no. 2, pp. 255–266, Nov. 2012, doi: 10.1515/plm-2012-0034.

[2] A. S. Hussain, H. S. Hussain, N. Betcher, R. Behm, and B. Cagir, "Proper use of noncontact infrared thermometry for temperature screening during COVID-19," *Sci. Rep.*, vol. 11, no. 1, p. 11832, Dec. 2021, doi: 10.1038/s41598-021-90100-1.

[3] M. Bardou, P. Seng, L. Meddeb, J. Gaudart, E. Honnorat, and A. Stein, "Modern approach to infectious disease management using infrared thermal camera scanning for fever in healthcare settings," *J. Infect.*, vol. 74, no. 1, pp. 95–97, Jan. 2017, doi: 10.1016/j.jinf.2016.08.017.

[4] S. De Bruyne, M. M. Speeckaert, and J. R. Delanghe, "Applications of mid-infrared spectroscopy in the clinical laboratory setting," *Crit. Rev. Clin. Lab. Sci.*, vol. 55, no. 1, pp. 1–20, Jan. 2018, doi: 10.1080/10408363.2017.1414142.

[5] R. Selvaraj, N. J. Vasa, S. M. S. Nagendra, and B. Mizaikoff, "Advances in Mid-Infrared Spectroscopy-Based Sensing Techniques for Exhaled Breath Diagnostics," *Molecules*, vol. 25, no. 9, p. 2227, May 2020, doi: 10.3390/molecules25092227.

[6] T. Koyama, N. Shibata, S. Kino, A. Sugiyama, N. Akikusa, and Y. Matsuura, "A Compact Mid-Infrared Spectroscopy System for Healthcare Applications Based on a Wavelength-Swept, Pulsed Quantum Cascade Laser," *Sensors*, vol. 20, no. 12, p. 3438, Jun. 2020, doi: 10.3390/s20123438.

[7] M. A. Naeser, M. D. Ho, P. I. Martin, M. R. Hamblin, and B.-B. Koo, "Increased Functional Connectivity Within Intrinsic Neural Networks in Chronic Stroke Following Treatment with Red/Near-Infrared Transcranial Photobiomodulation: Case Series with Improved Naming in Aphasia," *Photobiomodulation, Photomedicine, Laser Surg.*, vol. 38, no. 2, pp. 115–131, Feb. 2020, doi: 10.1089/photob.2019.4630.

[8] K.-S. Hong and M. A. Yaqub, "Application of functional near-infrared spectroscopy in the healthcare industry: A review," *J. Innov. Opt. Health Sci.*, vol. 12, no. 06, p. 1930012, Nov. 2019, doi: 10.1142/S179354581930012X.

[9] M. R. Hamblin, "Photobiomodulation for traumatic brain injury and stroke," *J. Neurosci. Res.*, vol. 96, no. 4, pp. 731–743, Apr. 2018, doi: 10.1002/jnr.24190.

[10] P. Jain, A. M. Joshi, and S. P. Mohanty, "iGLU: An Intelligent Device for Accurate Noninvasive Blood Glucose-Level Monitoring in Smart Healthcare," *IEEE Consum. Electron. Mag.*, vol. 9, no. 1, pp. 35–42, Jan. 2020, doi: 10.1109/MCE.2019.2940855.

[11] S. Badriah, Y. Bahtiar, and A. Andang, "Near Infrared LEDs-Based Non-Invasive Blood Sugar Testing for Detecting Blood Sugar Levels on Diabetic Care," *J. Biomimetics, Biomater. Biomed. Eng.*, vol. 55, pp. 183–191, Mar. 2022, doi: 10.4028/p-vthp40.
[12] B. Javid, F. Fotouhi-Ghazvini, and F. Zakeri, "Noninvasive optical diagnostic techniques for mobile blood glucose and bilirubin monitoring," *J. Med. Signals Sensors*, vol. 8, no. 3, p. 125, 2018, doi: 10.4103/jmss.JMSS_8_18.
[13] P. Pellicori *et al.*, "Non-invasive measurement of right atrial pressure by near-infrared spectroscopy: preliminary experience. A report from the SICA-HF study," *Eur. J. Heart Fail.*, vol. 19, no. 7, pp. 883–892, Jul. 2017, doi: 10.1002/ejhf.825.
[14] H. Xu, J. Liu, J. Zhang, G. Zhou, N. Luo, and N. Zhao, "Flexible Organic/Inorganic Hybrid Near-Infrared Photoplethysmogram Sensor for Cardiovascular Monitoring," *Adv. Mater.*, vol. 29, no. 31, pp. 1–6, 2017, doi: 10.1002/adma.201700975.
[15] A. Khaliduzzaman, S. Fujitani, A. Kashimori, T. Suzuki, Y. Ogawa, and N. Kondo, "A non-invasive diagnosis technique of chick embryonic cardiac arrhythmia using near infrared light," *Comput. Electron. Agric.*, vol. 158, no. February, pp. 326–334, Mar. 2019, doi: 10.1016/j.compag.2019.02.014.
[16] N. S. Ali, Z. A. A. Alyasseri, and A. Abdulmohson, "Real-Time Heart Pulse Monitoring Technique Using Wireless Sensor Network and Mobile Application," *Int. J. Electr. Comput. Eng.*, vol. 8, no. 6, p. 5118, Dec. 2018, doi: 10.11591/ijece.v8i6.pp5118-5126.
[17] G. Simone *et al.*, "High-Accuracy Photoplethysmography Array Using Near-Infrared Organic Photodiodes with Ultralow Dark Current," *Adv. Opt. Mater.*, vol. 8, no. 10, p. 1901989, May 2020, doi: 10.1002/adom.201901989.
[18] N. Hakimi, A. Jodeiri, M. Mirbagheri, and S. K. Setarehdan, "Proposing a convolutional neural network for stress assessment by means of derived heart rate from functional near infrared spectroscopy," *Comput. Biol. Med.*, vol. 121, no. May, p. 103810, Jun. 2020, doi: 10.1016/j.compbiomed.2020.103810.
[19] K. Oiwa, Y. Ozawa, K. Nagumo, S. Nishimura, Y. Nanai, and A. Nozawa, "Remote Blood Pressure Sensing Using Near-Infrared Wideband LEDs," *IEEE Sens. J.*, vol. 21, no. 21, pp. 24327–24337, Nov. 2021, doi: 10.1109/JSEN.2021.3111628.
[20] Y. Ozawa, K. Oiwa, S. Miyazaki, S. Nishimura, Y. Nanai, and A. Nozawa, "Improving the Accuracy of Noncontact Blood Pressure Sensing Using Near-Infrared Light," *IEEJ Trans. Electron. Inf. Syst.*, vol. 140, no. 7, pp. 769–774, Jul. 2020, doi: 10.1541/ieejeiss.140.769.
[21] G. Wang, M. Atef, and Y. Lian, "Towards a Continuous Non-Invasive Cuffless Blood Pressure Monitoring System Using PPG: Systems and Circuits Review," *IEEE Circuits Syst. Mag.*, vol. 18, no. 3, pp. 6–26, 2018, doi: 10.1109/MCAS.2018.2849261.
[22] V. P. Rachim, T. H. Huynh, and W.-Y. Chung, "Wrist Photo-Plethysmography and Bio-Impedance Sensor for Cuff-Less Blood Pressure Monitoring," in *2018 IEEE SENSORS*, Oct. 2018, vol. 2018-Octob, pp. 1–4. doi: 10.1109/ICSENS.2018.8589559.
[23] P. Bansal, M. Malik, and R. Kundu, "Smart heart rate monitoring system," in *2018 IEEMA Engineer Infinite Conference (eTechNxT)*, Mar. 2018, pp. 1–4. doi: 10.1109/ETECHNXT.2018.8385347.
[24] D. Biswas, N. Simoes-Capela, C. Van Hoof, and N. Van Helleputte, "Heart Rate Estimation From Wrist-Worn Photoplethysmography: A Review," *IEEE Sens. J.*, vol. 19, no. 16, pp. 6560–6570, Aug. 2019, doi: 10.1109/JSEN.2019.2914166.
[25] K. Matsumura, S. Toda, and Y. Kato, "RGB and Near-Infrared Light Reflectance/Transmittance Photoplethysmography for Measuring Heart Rate During Motion," *IEEE Access*, vol. 8, pp. 80233–80242, 2020, doi: 10.1109/ACCESS.2020.2990438.
[26] I. Lee, N. Park, H. Lee, C. Hwang, J. H. Kim, and S. Park, "Systematic Review on Human Skin-Compatible Wearable Photoplethysmography Sensors," *Appl. Sci.*, vol. 11, no. 5, p. 2313, Mar. 2021, doi: 10.3390/app11052313.
[27] A. Hina and W. Saadeh, "A Noninvasive Glucose Monitoring SoC Based on Single

Wavelength Photoplethysmography," *IEEE Trans. Biomed. Circuits Syst.*, vol. 14, no. 3, pp. 504–515, Jun. 2020, doi: 10.1109/TBCAS.2020.2979514.

[28] S. Ramasahayam, L. Arora, and S. R. Chowdhury, "FPGA Based Smart System for Non Invasive Blood Glucose Sensing Using Photoplethysmography and Online Correction of Motion Artifact," in *Smart Sensors, Measurement and Instrumentation*, vol. 22, 2017, pp. 1–21. doi: 10.1007/978-3-319-47319-2_1.

[29] Y. (Joseph) Segman, "Device and Method for Noninvasive Glucose Assessment," *J. Diabetes Sci. Technol.*, vol. 12, no. 6, pp. 1159–1168, Nov. 2018, doi: 10.1177/1932296818763457.

[30] M. Strik *et al.*, "Smartwatch-based detection of cardiac arrhythmias: Beyond the differentiation between sinus rhythm and atrial fibrillation," *Hear. Rhythm*, vol. 18, no. 9, pp. 1524–1532, Sep. 2021, doi: 10.1016/j.hrthm.2021.06.1176.

[31] J. Yadav, A. Rani, V. Singh, and B. M. Murari, "Comparative Study of Different Measurement Sites Using NIR Based Non-invasive Glucose Measurement System," *Procedia Comput. Sci.*, vol. 70, pp. 469–475, 2015, doi: 10.1016/j.procs.2015.10.082.

[32] A. Kassem, M. Hamad, G. G. Harbieh, and C. El Moucary, "A Non-Invasive Blood Glucose Monitoring Device," in *2020 IEEE 5th Middle East and Africa Conference on Biomedical Engineering (MECBME)*, Oct. 2020, vol. 2020-Octob, no. 978, pp. 1–4. doi: 10.1109/MECBME47393.2020.9265170.

[33] E. Sazonov, *WEARABLE SENSORS Fundamentals, Implementation and Applications*, 2nd editio., no. July. Elsevier, 2021.

[34] M. R. Haque, S. M. T. Uddin Raju, M. A.-U. Golap, and M. M. A. Hashem, "Corrections to 'A Novel Technique for Non-Invasive Measurement of Human Blood Component Levels From Fingertip Video Using DNN Based Models,'" *IEEE Access*, vol. 9, pp. 84178–84179, 2021, doi: 10.1109/ACCESS.2021.3087280.

[35] V. Periyasamy, M. Pramanik, and P. K. Ghosh, "Review on Heart-Rate Estimation from Photoplethysmography and Accelerometer Signals During Physical Exercise," *J. Indian Inst. Sci.*, vol. 97, no. 3, pp. 313–324, Sep. 2017, doi: 10.1007/s41745-017-0037-1.

[36] A. Kamišalić, I. Fister, M. Turkanović, and S. Karakatič, "Sensors and Functionalities of Non-Invasive Wrist-Wearable Devices: A Review," *Sensors*, vol. 18, no. 6, p. 1714, May 2018, doi: 10.3390/s18061714.

[37] F. J. Velez and Fardin Derogarian Miyandoab, *Wearable Technologies and Wireless Body Sensor Networks for Healthcare*. Institution of Engineering and Technology, 2019. [Online]. Available: https://digital-library.theiet.org/content/books/10.1049/pbhe011e_ch2

[38] L. Adhikari and S. K. Pahuja, "Mathematical Modeling and Simulation of Photoplethysmography," in *2020 International Conference on Communication and Signal Processing (ICCSP)*, Jul. 2020, pp. 1307–1311. doi: 10.1109/ICCSP48568.2020.9182070.

[39] Maxim Integrated, "MAX30102 - High-Sensitivity Pulse Oximeter and Heart-Rate Sensor for Wearable Health," 2015. [Online]. Available: https://www.maximintegrated.com/en/products/sensors/MAX30102.html

[40] M. A. Motin, P. P. Das, C. K. Karmakar, and M. Palaniswami, "Compact Pulse Oximeter Designed for Blood Oxygen Saturation and Heart Rate Monitoring," in *2021 3rd International Conference on Electrical & Electronic Engineering (ICEEE)*, Dec. 2021, pp. 125–128. doi: 10.1109/ICEEE54059.2021.9718773.

[41] L. Fiorini, F. Cavallo, M. Martinelli, and E. Rovini, "Characterization of a PPG Wearable Sensor to Be Embedded into an Innovative Ring-Shaped Device for Healthcare Monitoring," in *Lecture Notes in Electrical Engineering*, vol. 725, 2021, pp. 49–63. doi: 10.1007/978-3-030-63107-9_5.

[42] R. Kopel *et al.*, "No time for drifting: Comparing performance and applicability of signal detrending algorithms for real-time fMRI," *Neuroimage*, vol. 191, no. February, pp. 421–429, May 2019, doi: 10.1016/j.neuroimage.2019.02.058.

[43] X. Dong, G. Li, Y. Jia, B. Li, and K. He, "Non-iterative denoising algorithm for mechanical

vibration signal using spectral graph wavelet transform and detrended fluctuation analysis," *Mech. Syst. Signal Process.*, vol. 149, p. 107202, Feb. 2021, doi: 10.1016/j.ymssp.2020.107202.

[44] G. Georgieva-Tsaneva, E. Gospodinova, M. Gospodinov, and K. Cheshmedzhiev, "Portable Sensor System for Registration, Processing and Mathematical Analysis of PPG Signals," *Appl. Sci.*, vol. 10, no. 3, p. 1051, Feb. 2020, doi: 10.3390/app10031051.

[45] M. S. Milivojevic, A. Gavrovska, I. Reljin, and B. Reljin, "Using Optical IoT Sensing for Detrended Fluctuation Analysis of Skin Blood Pulsation during Visual Stimulation Task," in *2019 27th Telecommunications Forum (TELFOR)*, Nov. 2019, pp. 1–4. doi: 10.1109/TELFOR48224.2019.8971288.

[46] S. Rajala, H. Lindholm, and T. Taipalus, "Comparison of photoplethysmogram measured from wrist and finger and the effect of measurement location on pulse arrival time," *Physiol. Meas.*, vol. 39, no. 7, p. 075010, Aug. 2018, doi: 10.1088/1361-6579/aac7ac.

[47] P.-Y. Tsai *et al.*, "Coherence between Decomposed Components of Wrist and Finger PPG Signals by Imputing Missing Features and Resolving Ambiguous Features," *Sensors*, vol. 21, no. 13, p. 4315, Jun. 2021, doi: 10.3390/s21134315.

92_Revisi_2.0.docx

ORIGINALITY REPORT

13%	10%	7%	4%
SIMILARITY INDEX	INTERNET SOURCES	PUBLICATIONS	STUDENT PAPERS

PRIMARY SOURCES

1	www.semanticscholar.org Internet Source	4%
2	www.tandfonline.com Internet Source	1%
3	Xin Dong, Guolong Li, Yachao Jia, Biao Li, Kun He. "Non-iterative denoising algorithm for mechanical vibration signal using spectral graph wavelet transform and detrended fluctuation analysis", Mechanical Systems and Signal Processing, 2021 Publication	1%
4	doaj.org Internet Source	1%
5	essay.utwente.nl Internet Source	1%
6	scholarworks.sjsu.edu Internet Source	1%
7	ijhss.net Internet Source	1%

8	Submitted to University of Alabama at Birmingham Student Paper	<1%
9	Siti Badriah, Yanyan Bahtiar, Asep Andang. "Near Infrared LEDs-Based Non-Invasive Blood Sugar Testing for Detecting Blood Sugar Levels on Diabetic Care", Journal of Biomimetics, Biomaterials and Biomedical Engineering, 2022 Publication	<1%
10	"XLV Mexican Conference on Biomedical Engineering", Springer Science and Business Media LLC, 2023 Publication	<1%
11	Submitted to University of Nottingham Student Paper	<1%
12	cronfa.swan.ac.uk Internet Source	<1%
13	Elena Miller. "The Relationship Between Emotional Intelligence and Clinical Success at the Completion of One Year of Courses for Diagnostic Medical Sonography or Radiography Students", Journal of Diagnostic Medical Sonography, 2022 Publication	<1%
14	I. Pomeranz, S.M. Reddy. "On diagnosis and diagnostic test generation for pattern-	<1%

	dependent transition faults", IEEE Transactions on Computer-Aided Design of Integrated Circuits and Systems, 2001 Publication	
15	repo.poltekkestasikmalaya.ac.id Internet Source	<1 %
16	core.ac.uk Internet Source	<1 %
17	Lalita Adhikari, Sharvan Kumar Pahuja. "Mathematical Modeling and Simulation of Photoplethysmography", 2020 International Conference on Communication and Signal Processing (ICCSP), 2020 Publication	<1 %
18	www.maximintegrated.com Internet Source	<1 %
19	idoc.pub Internet Source	<1 %
20	Submitted to Rochester Institute of Technology Student Paper	<1 %
21	Submitted to University of Auckland Student Paper	<1 %
22	"Proceedings of the 21st Congress of the International Ergonomics Association (IEA	<1 %

2021)", Springer Science and Business Media LLC, 2021
Publication

23	Júlio C. Costa, Filippo Spina, Pasindu Lugoda, Leonardo Garcia-Garcia, Daniel Roggen, Niko Münzenrieder. "Flexible Sensors—From Materials to Applications", Technologies, 2019 Publication	<1 %
24	www.diva-portal.org Internet Source	<1 %
25	www.researchgate.net Internet Source	<1 %

Exclude quotes	Off	Exclude matches	Off
Exclude bibliography	On		